HHS Public Access

Author manuscript

Biol Psychiatry. Author manuscript; available in PMC 2023 November 15.

Published in final edited form as:

Biol Psychiatry. 2022 November 15; 92(10): 815–826. doi:10.1016/j.biopsych.2021.04.023.

CYFIP1 dosages exhibit divergent behavioral impact via diametric regulation of NMDAR complex translation in mouse models of psychiatric disorders

Nam-Shik Kim[#1,11], **Francisca Rojas Ringeling**[#2,3], **Ying Zhou**[2], **Ha Nam Nguyen**[2], **Stephanie J. Temme**[1], **Yu-Ting Lin**[2], **Stephen Eacker**[2], **Valina L. Dawson**[2,4], **Ted M. Dawson**[2,4], **Bo Xiao**[4,12], **Kuei-sen Hsu**[5], **Stefan Canzar**[3], **Weidong Li**[6], **Paul Worley**[4], **Kimberly M. Christian**[1], **Ki-Jun Yoon**[1,11,#], **Hongjun Song**[1,7,8,9], **Guo-li Ming**[1,7,8,10,#]

[1]Department of Neuroscience and Mahoney Institute for Neurosciences, University of Pennsylvania, Philadelphia, PA 19104, USA.

[2]Institute for Cell Engineering, Johns Hopkins University School of Medicine, Baltimore, MD 21205, USA

[3]Gene Center, Ludwig-Maximilians-Universität München, Munich 81377, Germany.

[4]The Solomon H Snyder Department of Neuroscience, Johns Hopkins University School of Medicine, Baltimore, MD 21205, USA.

[5]Department of Pharmacology, College of Medicine, National Cheng Kung University, Tainan 701, Taiwan.

[6]Bio-X Institutes, Key Laboratory for the Genetics of Development and Neuropsychiatric Disorders, Shanghai Jiao Tong University, Shanghai 200030, China.

[7]Department of Cell and Developmental Biology, University of Pennsylvania, Philadelphia, PA 19104, USA.

[8]Institute for Regenerative Medicine, University of Pennsylvania, Philadelphia, PA 19104, USA.

[9]The Epigenetics Institute, University of Pennsylvania, Philadelphia, PA 19104, USA.

[10]Department of Psychiatry, Perelman School for Medicine, University of Pennsylvania, Philadelphia, PA 19104, USA.

[#]Correspondence should be addressed to: gming@pennmedicine.upenn.edu (+1 215-573-2449; G-l.M), and kijunyoon@kaist.ac.kr (+82 42-350-2628; K.-J.Y).

CONTRIBUTIONS

N-S. K. and F.R.R. contributed equally to this work. N-S.K. and K-J.Y. generated the cKO and cOE mice and performed the behavioral and biochemical analyses. F.R.R. and S.C. contributed to RIP-seq and analysis. Y.Z., W.L. and K.M.C. contributed to behavioral analysis. H.N.N. contributed to iPSC experiments. S.T., Y-T.L., and K-s. H. contributed to electrophysiological recording. S.E., V.L.D., and T.M.D. contributed to sucrose gradient experiments, B.X. and P.W. contributed to cOE mouse line generation. N-S.K., K-J.Y., H.S. and G-l.M. conceived the project and wrote the manuscript with inputs from all authors.

DISCLOSURES

The authors report no biomedical financial interests or potential conflicts of interest.

[11]Current address: Department of Biological Sciences, Korea Advanced Institute of Science and Technology (KAIST), Daejeon 34141, Republic of Korea.

[12]Current address: Department of Biology, Southern University of Science and Technology, Shenzhen 518000, Guangdong, China.

[#] These authors contributed equally to this work.

Abstract

BACKGROUND: Gene dosage imbalance caused by copy number variations (CNVs) are prominent contributors to brain disorders. 15q11.2 CNV duplications and deletions have been associated with autism spectrum disorder (ASD) and schizophrenia (SCZ), respectively. The mechanism underlying these diametric contributions remains unclear.

METHODS: We established both loss-of-function and gain-of-function mouse models of *Cyfip1,* one of four genes within 15q11.2 CNVs. To assess the functional consequences of altered CYFIP1 levels, we performed systematic investigations on behavioral, electrophysiological, and biochemical phenotypes in both mouse models. In addition, we utilized RNA immunoprecipitation (RIP)-seq analysis to reveal molecular targets of CYFIP1 *in vivo*.

RESULTS: *Cyfip1* loss-of-function and gain-of function mouse models exhibited distinct and shared behavioral abnormalities related to ASD and SCZ. RIP-seq analysis identified mRNA targets of CYFIP1 *in vivo*, including postsynaptic NMDA receptor (NMDAR) complex components. In addition, these mouse models showed diametric changes in levels of postsynaptic NMDAR complex components at synapses due to dysregulated protein translation, resulting in bidirectional alteration of NMDAR-mediated signaling. Importantly, pharmacological balancing of NMDAR signaling in these mouse models with diametric *CYFIP1* dosages rescues behavioral abnormalities.

CONCLUSIONS: CYFIP1 regulates protein translation of NMDAR and associated complex components at synapses to maintain normal synaptic functions and behaviors. Our integrated analyses provide insight into how gene dosage imbalance caused by CNVs may contribute to divergent neuropsychiatric disorders.

Keywords

Gene dosage; autism spectrum disorder; schizophrenia; synaptic protein translation; NMDA receptor; RNA binding protein

INTRODUCTION

Mental disorders such as schizophrenia (SCZ) and autistic spectrum disorder (ASD) are chronic and disabling. A large number of susceptibility genes for ASD and SCZ have been identified from human genetic studies, and various experimental models are being developed to investigate how these susceptibility genes regulate behavior (1, 2). In addition to single-nucleotide polymorphisms or mutations in individual genes, submicroscopic variations in DNA copy number (CNV) are also widespread in human genomes, and specific CNVs have been identified as significant risk factors for ASD and SCZ (3). Moreover, aggregate data

have provided support for the polygenic inheritance and genetic overlap between SCZ and ASD (4–7). Intriguingly, diametric dosages of the same mutations (deletion vs. duplication), including both individual genes (e.g. *MeCP2*, *SHANK3*) and CNVs (e.g. 15q11.2, 16p11.2, 22q11.2), lead to divergent brain disorders (8). The underlying mechanism is unknown.

15q11.2 CNVs have emerged as prominent genetic risk factors for various neuropsychiatric disorders, including ASD, SCZ and intellectual disability (9–12). Specifically, 15q11.2 microduplications have been associated with ASD (13, 14), whereas microdeletions of the same region have been identified as one of the three most frequent CNV risk factors for SCZ (15). Even non-diagnosed carriers of 15q11.2 microdeletions showed cognitive function that was in between neurotypical controls and SCZ patients (16–18). 15q11.2 microdeletion and microduplication also result in reciprocal effects on the volume of some human brain regions, including gray matter in the perigenual anterior cingulated cortex and white matter in the temporal lobe (16, 18–20) It remains unclear how different doses of genes within the 15q11.2 region may contribute to the etiopathology underlying divergent neuropsychiatric disorders.

CYFIP1 is one of the four genes within 15q11.2 and encodes a protein that interacts with fragile X mental retardation protein (FMRP) and eukaryotic translation initiation factor 4E (eIF4E) and negatively regulates mRNA translation at synapses in an activity-dependent manner (21, 22). An altered level of CYFIP1 leads to abnormalities in dendrite complexity and spine morphology (23–25), synaptic function (26, 27), and behavior (25, 28–32). Moreover, common SNPs in *CYFIP1* have been associated with SCZ (33) and ASD (34), and *CYFIP1* mRNA expression is increased in ASD patients (35, 36). These findings highlight *CYFIP1* as the most compelling genetic risk factor for neuropsychiatric disorders within the 15q11.2 region. Thus, an increase or decrease in CYFIP1 levels may lead to diametric alterations in common signaling pathways, which could be the underlying mechanism for the pathogenesis of the 15q11.2 CNV-mediated risk for neuropsychiatric disorders. However, mRNA targets of CYFIP1 and effects of the CYFIP1 dosage on the protein translation of those targets have not been examined in a non-biased manner.

To understand how different dosages of *CYFIP1* may lead to divergent brain disorders, we established both loss-of-function and gain-of-function mouse models of *Cyfip1*. Interestingly, the loss of *Cyfip1* model exhibited distinct behavioral abnormalities related to SCZ, whereas the gain of *Cyfip1* model exhibited ASD-related behavioral phenotypes. Mechanistically, genome-wide RIP-seq identified novel CYFIP1-associated mRNA targets related to synaptic function, postsynaptic density and the NMDA receptor complex. Furthermore, these mouse models showed dysregulation of postsynaptic protein translation on specific targets of CYFIP1 and diametric changes in the levels of postsynaptic NMDAR complex components and signaling at synapses. Importantly, bidirectional pharmacological manipulations to re-balance NMDAR signaling largely rescue the behavioral abnormalities of these mouse models. Our integrated study provides insight into how 15q11.2 CNVs may contribute to divergent neuropsychiatric disorders.

METHODS AND MATERIALS

See Supplemental Methods and Materials for a detailed description of experimental methods and key Resource Table for materials.

Animals

The loss-of-function (cKO) and gain-of-function (cOE) mice were generated by the Transgenic Core Laboratory at Johns Hopkins School of Medicine (Figure S1). Both cKO and cOE mice were crossed with *Nestin-Cre* mice and they were backcrossed to C57BL/6J at least 6 times before all experiments. For most behavioral experiments, 3–4 month-old male mice were used. In the marble burying assay, nest building assay and pup retrieval assay, 3–4 month-old female mice were used. All mouse work was performed with protocols approved by the Animal Care and Use Committee of Johns Hopkins University School of Medicine and University of Pennsylvania.

Data and code availability

The GEO accession number for the RIP-seq dataset is GSE166939.

RESULTS

Loss of CYFIP1 function results in behavioral abnormalities related to schizophrenia

To investigate the *in vivo* effects of differential *Cyfip1* dosages on animal behavior under the same conditions, we generated a conditional knockout mouse model (*Nestin*-Cre:*Cyfip1*$^{\text{floxed/floxed}}$, named cKO) and a conditional overexpression mouse model of *Cyfip1* (*Nestin*-Cre: *ROSA26*$^{Cyfip1\ \text{KI/KI}}$, named cOE). cKO showed complete ablation of the CYFIP1 protein in forebrain lysates after E17.5 (Figure S1C). On the other hand, the homozygote cOE mice showed about 1.5–2 fold increase of CYFIP1 protein levels in the adult hippocampus and cortex (Figure S1F), similar to ASD patients with 15q11.2 duplication (14). We used the homozygote cOE mice for all analyses. The cKO and cOE mice were fertile, and displayed a normal appearance and expected Mendelian ratio of genotypes in adulthood (data not shown).

We first tested cKO mice with a battery of behavioral analyses related to human mental disorders. cKO mice displayed normal locomotor activity, motor coordination, nociception response, novel object recognition and repetitive behaviors (Figure S2A–E and Table S1). To test whether cKO mice exhibit behavioral abnormalities related to negative symptoms in SCZ, we first performed a three-chamber social interaction assay (37). cKO mice showed a similar preference for a mouse (stranger 1) over an empty cage in comparison with littermate wild-type mice (*Cyfip1*$^{\text{floxed/floxed}}$, named WT1; Figure 1A). However, when the empty cage was replaced by a novel mouse (stranger 2), cKO mice did not show a significant preference for stranger 2 over stranger 1, while WT1 mice preferred to interact with stranger 2 (Figure 1B), indicating impaired social novelty recognition. Moreover, cKO mice exhibited impaired prepulse inhibition (PPI) and an elevated startle response (Figure 1C–D), suggesting deficits in sensorimotor gating commonly found in SCZ patients. In addition, cKO mice showed

elevated behavioral despair with increased immobility in both the tail suspension test (TST) and forced swim test (FST) compared with WT1 mice (Figure 1E–F).

We also measured amphetamine-induced hyperactivity, which is widely used in animals to model neuropsychiatric disorders and positive symptoms of SCZ (38). cKO mice showed increased locomotor activity after an acute injection of amphetamine compared to the WT1 mice (Figure 1G). The *Nestin-Cre* transgene did not affect social interaction, amphetamine-induced hyperactivity, or prepulse inhibition (Figure S2F–I).

In summary, these results suggest that the *Cyfip1* loss-of-function in mice leads to multiple behavioral abnormalities related to negative and positive symptoms of SCZ patients.

Increased *Cyfip1* dosage leads to behavioral abnormalities related to ASD

Given that *CYFIP1* mRNA expression is significantly upregulated in ASD patients (14, 24, 36), we examined whether overexpression of CYFIP1 may result in ASD-related behavioral abnormalities. cOE mice displayed normal locomotor activity and novel object recognition (Figure S3A–B and Table S1). Interestingly, in the first stage of the three-chamber social interaction assay, cOE mice exhibited decreased interaction with stranger 1 compared with littermate wild-type mice (*ROSA26*$^{Cyfip1\ KI/KI}$, named WT2; Figure 2A). cOE mice also did not prefer to interact with a novel mouse (stranger 2), whereas the WT2 mice interacted significantly more with stranger 2 than with stranger 1 (Figure 2B). These results suggest that cOE mice have an impaired social approach and social novelty recognition. Repetitive and stereotyped patterns of behavior are one of the core behavioral domains for the ASD diagnosis (39). We assessed repetitive behaviors of cOE mice with the marble burying assay and measuring digging behavior (40). cOE mice buried significantly more marbles compared to the WT2 mice (Figure 2C). Moreover, cOE mice also spent more time engaged in digging behavior compared to the WT2 mice (Figure 2D).

Maternal behaviors are frequently impaired in mouse models of ASD (41–43). The survival rate of pups from cOE dams was markedly lower than that from WT2 dams (Figure 2E). At postnatal day 3, some of the pups from cOE dams did not show milk in their stomachs, whereas milk was observed in the stomachs of all pups from WT2 dams (Figure S3C). As a result, the number of surviving pups at postnatal day 7 from cOE dams was significantly smaller compared with that from WT2 dams (Figure 2E and S3D). Among surviving pups from cOE dams, the number of cOE and WT pups was similar, suggesting that impaired maternal care is not dependent on genotypes of the pups (data not shown). Moreover, cOE females showed impaired nest building behaviors (Figure 2F) and less efficient pup retrieval compared with WT2 females (Figure 2G), suggesting that multiple traits of maternal behaviors are impaired with an increased *Cyfip1* dosage in a mouse model. On the other hand, cKO dams showed similar levels in the pup survival rate with the WT1 dams (data not shown). In addition, similar to cKO mice, cOE mice displayed increased amphetamine-induced hyperactivity compared to the WT2 mice, indicating dysfunction in the dopaminergic system of the cOE mice (Figure 2H). Unlike with cKO mice, cOE mice did not display elevated despair in the TST (Figure S3E), or abnormal sensorimotor gating in the PPI (Figure S3F and Table S1). Taken together, our behavioral analyses of cOE mice showed that increased *Cyfip1* dosage results in several behavioral abnormalities related to

ASD, including social impairment, increased repetitive behaviors and abnormal maternal behaviors.

CYFIP1 interacts with mRNAs encoding synaptic and NMDA receptor complex-related proteins in the mouse hippocampus and human cortical tissue

CYFIP1 regulates mRNA translation in neurons (21, 22). To identify which mRNAs are the potential targets of CYFIP1 for translation regulation, we performed RNA immunoprecipitation sequencing (RIP-seq) (44) of the adult mouse hippocampus. We took advantage of our cOE mouse model, which expresses an HA-tagged CYFIP1 (Figure S1D), enabling us to immunoprecipitate CYFIP1 and associated mRNA using an anti-HA antibody with high specificity (Figure 3A–B). We identified 1,721 transcripts that were found to be enriched in 3 out of 4 comparisons with controls (Table S2). Gene ontology analysis showed significant enrichment of terms related to neuronal and synaptic components and processes, and more specifically to the NMDAR complex (Figure 3C–D and Table S3). Disease ontology analysis revealed enrichment for neuropsychiatric diseases, including SCZ and ASD (Figure 3D and Table S3).

To confirm the interaction between the CYFIP1 protein and some of the targets identified by our genome-wide analysis, we performed immunoprecipitation of endogenous CYFIP1 with an anti-CYFIP1 antibody using hippocampal tissue from the wild-type mice, followed by quantitative PCR (RIP-qPCR). We chose several mRNAs related to the NMDAR complex for further validation and indeed found that their mRNAs were enriched in the anti-CYFIP1 pulled-down samples compared with the IgG pulled-down samples, including *Shank1*, *Shank2*, *Grin2a*, *Grin2b*, and *Gabbr2* (Figure 3E). To explore whether these interactions are conserved in the human brain, we performed RIP-qPCR experiments using surgical adult human cortical tissues. We found that indeed they were also significantly enriched in the cerebral cortex samples pulled-down with an anti-CYFIP1 antibody compared to the IgG pull down (Figure 3F).

Given that CYFIP1 interacts with FMRP, we compared mRNA targets of these two proteins. Between 1,721 CYFIP1 targets we identified and 842 FMRP targets previously reported (45), only 130 mRNA targets were shared (Table S4), suggesting independent direct regulation of many mRNA targets by CYFIP1 and FMRP.

CYFIP1 regulates mRNA translation of NMDAR subunits and associated complex

CYFIP1 represses the translation of its target mRNAs by inhibiting the interaction between eIF4E and eIF4G at the 5’ cap structure (21, 22, 46). The mRNA levels encoding the NMDAR subunits and associated complex proteins were not changed in either cKO or cOE mice (Figure S4A–B), indicating that CYFIP1 may not regulate transcription or the stability of these mRNA targets. To explore whether altered CYFIP1 dosages lead to dysregulated protein translation of CYFIP1 target mRNAs, we applied the PUNCH-P technique (47) to monitor the amount of nascent peptides from cKO and cOE hippocampi (Figure 4A). To determine effects of CYFIP1 ablation on the general translation rate, the amount of total biotin-puromycin labeled nascent peptides were accessed by streptavidin-HRP immunoblotting. Similar amounts of peptides were being synthesized in cKO mice

compared to WT1 mice, suggesting the loss of CYFIP1 function does not change the general translation rate (Figure 4B). To monitor the protein translation rate of specific target mRNAs, biotin-puromycin labeled peptides were captured and purified by streptavidin beads and examined by specific antibodies. The protein synthesis of postsynaptic NMDAR subunits and associated complex components, but not presynaptic protein SYN1, was significantly increased in the cKO mice compared to the WT1 mice (Figure 4C). Conversely, the amount of protein synthesis from those transcripts was substantially lower in cOE mice compared to WT2 mice (Figure 4D).

To confirm our results, we performed polysome profile analysis with hippocampal lysates. The general polysome profile was not significantly altered in cKO mice compared to WT1 mice (Figure S4C), consistent with the unchanged general translation rate revealed by PUNCH-P (Figure 4B). Notably, *Grin2b* and *Shank2* mRNA distributions were shifted to heavier polysome fractions in cKO mice compared with WT1 mice (Figure S4C and S4E), indicating an enhanced translation efficiency. On the other hand, *Grin2b* and *Shank2* mRNA distributions were shifted to the lighter fractions in cOE mice compared with WT2 mice (Figure S4D and S4F), indicating repressed translation of those mRNAs. These results suggest that the balanced level of CYFIP1 protein is important for translational regulation of its target mRNAs.

Protein expression of the NMDAR-associated complex and postsynaptic scaffolding are altered in the synaptosome depending on *CYFIP1* dosages

To examine changes in protein expression at synapses of cKO and cOE mice, including the CYFIP1-interacting mRNA targets identified by RIP-seq analysis, synaptosomes were isolated from the hippocampi for Western blotting analysis (Figure S5A). As expected, the expression of CYFIP1 was completely abolished in the cKO hippocampus and increased in the cOE hippocampus (Figure 5A–B). Interestingly, the expression levels of the NMDAR subunits (GRIN1 and GRIN2B) and NMDAR-associated postsynaptic scaffolding proteins (SHANK2 and PSD95) (48) were significantly increased in the cKO synaptosomes (Figure 5A). In contrast, expression levels of NMDAR subunits (GRIN1, GRIN2A, and GRIN2B), SHANK2 and PSD95 were reduced in the cOE synaptosome compared with the WT2 synaptosome (Figure 5B), suggesting a reciprocal regulation of postsynaptic proteins dependent on different CYFIP1 dosages. The expression levels of the AMPAR subunits, presynaptic proteins, and Homer1 were unchanged both in the cKO and cOE hippocampi. Different from previous reports (21, 22), we did not observe any significant changes in the expression of ARC in our models (Figure 5A–B).

To examine whether similar regulation occurs in human models, we used patient induced pluripotent stem cell (iPSC) lines we previously generated from subjects with 15q11.2del CNVs and control subjects (49). Western blot analyses of cortical neurons differentiated from these iPSC lines also showed increased levels of GRIN2B proteins in both the whole cell lysate and synaptosomes (Figure S5B–C).

Imbalanced CYFIP1 expression results in reciprocal alterations in NMDAR functions

Dysfunction in NMDARs at synapses is associated with various neuropsychiatric disorders (43, 50–52). To examine whether the altered molecular composition of synapses at the postsynaptic site influences the function of NMDAR in cKO and cOE mice, we compared the relative contribution of the NMDA versus AMPA receptors to evoke EPSCs using whole-cell patch-clamp recordings from dentate gyrus granule cells in acute hippocampal slices. Consistent with the reciprocal protein expression of the NMDAR subunits in the hippocampi of cKO and cOE mice (Figure 5A–B), we found an increased NMDA/AMPA ratio in cKO mice, but a decreased NMDA/AMPA ratio in cOE mice compared to their wildtype littermates (Figure 6A–B).

Locomotor hyperactivity induced by systemic administration of an NMDAR antagonist has been used as an *in vivo* measurement of central neurotransmitter system activity (38, 53). Systemic injection of MK-801, a noncompetitive NMDAR antagonist, increased locomotor activity in both genotypes, but the levels of hyperactivity were significantly higher in cKO mice compared to WT1 mice (Figure 6C, top panel). Conversely, cOE mice showed a decreased level of hyperactivity compared to WT2 mice (Figure 6C, lower panel), suggesting reciprocal sensitivities for MK-801 in cKO and cOE mice.

Activation of NMDAR results in the upregulation of diverse downstream signaling events which are critical for synaptic function, such as phosphorylation of CaMKIIα (54) and p38 MAPK (55). We examined the perturbation of NMDAR downstream signaling due to alterations of the NMDAR activity in cKO and cOE mice. The levels of phosphorylation for CaMKIIα and p38 MAPK were higher in synaptosomes from hippocampi of cKO versus WT1 mice, but lower in cOE versus WT2 mice (Figure 6D).

Together, these results show that synaptic NMDAR function and downstream signaling are reciprocally impaired in opposite directions, depending on CYFIP1 levels in each mouse model.

Bidirectional modulation of NMDAR signaling rescues behavioral abnormalities in cKO and cOE mice

Imbalance in NMDAR signaling has been implicated in multiple neuropsychiatric disorders (51, 52). Since our mouse models showed bidirectional dysfunction in NMDAR signaling upon different *Cyfip1* dosages, we hypothesized that re-balancing NMDAR activity by reducing it in cKO mice and enhancing it in cOE mice may rescue the behavioral abnormalities in these models (Figure 7A). First, we treated cKO mice with the NMDAR antagonist memantine (56–59), which effectively normalized the augmented synaptic NMDAR signaling in cKO mice (Figure S6A). Indeed, the memantine treatment rescued the elevated behavioral despair of cKO mice in both the TST and FST (Figure 7B–C). In addition, the increased amphetamine-induced hyperactivity of cKO mice was also normalized with the memantine treatment (Figure 7D). On the other hand, impaired sensorimotor gating assessed by PPI in cKO mice was not improved with the memantine treatment (Figure S6B).

Next, we took advantage of a partial agonist of NMDAR, D-cycloserine (DCS), which has been shown to rescue ASD-related behaviors in animal models with reduced NMDAR function (43, 60). In the three-chamber social interaction assay, reduced social interaction and impaired social novelty recognition of cOE mice was improved by the DCS treatment (Figure 7E–F). In addition, the increased amphetamine-induced hyperactivity of cOE was restored by the DCS treatment (Figure 7G). The repetitive behaviors of cOE mice assessed by the marble burying assay were not rescued by the DCS treatment (data not shown).

In summary, bidirectional modulation to re-balance NMDAR function in cKO and cOE mice successfully rescued some behavioral abnormalities related to psychiatric disorders, implying that dysregulation of the NMDAR complex by abnormal levels of CYFIP1 is responsible for the abnormal behaviors in our animal models.

DISCUSSION

Balanced action of molecular regulators is essential to maintain the homeostatic control of the brain. Hence, either loss or gain of molecular functions can be deleterious to the nervous system (8). CNVs associated with neuropsychiatric disorders are one of the mechanisms by which an altered gene dosage can cause the failure of neuronal homeostasis. Although genetic studies have revealed significant overlap of genetic risk factors among mental disorders, it is not clear how an altered dosage of the same gene may contribute to different brain disorders. In this study, we generated new mouse models with nervous system-specific loss- or gain-of-function of RNA binding protein CYFIP1, a genetic risk factor both for SCZ and ASD. These mouse models displayed both distinct and shared behavioral abnormalities related to human mental disorders (Table S1). Notably, previous gain- or loss-of-function CYFIP1 rodent models generated by different strategies showed both similar and distinct behavioral phenotypes compared to our models (25, 28–30, 32) (Table S1). To investigate the underlying molecular mechanism, we identified novel CYFIP1-associated mRNA targets related to synaptic function, postsynaptic density and NMDAR complex by genome-wide RIP-seq analysis. Protein translation of CYFIP1 targets, including the NMDAR-associated complex, are diametrically altered upon loss or gain of CYFIP1 function. As a result, protein levels of CYFIP1 targets at synapses are dysregulated without a change in their mRNA expression depending on the level of CYFIP1 in the mouse models. Our study provides one explanation of how the action of a RNA binding protein can modulate the balance of protein translation and levels at synapses, which is essential to maintain typical behavioral responses.

Abnormal protein synthesis disrupts synaptic function and neuronal networks underlying the pathophysiology of mental disorders. Accordingly, translational machinery and their regulatory components have been frequently identified as risk factors for mental disorders. For example, the mTOR pathway is strongly associated with ASD, and its perturbation in mouse models leads to the core phenotypes of ASD (61–63). Exaggerated cap-dependent protein translation causes synaptic and behavioral abnormalities associated with ASD (64, 65), suggesting aberrant general protein translation is an important molecular process for ASD development. On the other hand, recent studies showed that SCZ patient-derived neural cells exhibit dysregulated protein translation and translational machinery, suggesting

translational control may be involved in the disease progression of SCZ (66, 67). However, molecular regulators that may explain the dysregulation of protein translation in both SCZ and ASD are unclear. In our study, we identified a set of novel mRNA targets interacting with CYFIP1 that are related to synaptic function. We also found that the protein levels of CYFIP1 targets at synapses are diametrically regulated, depending on the level of CYFIP1. Intriguingly, the impact appears to be specific to CYFIP1 targets as the total protein levels of AMPA receptors and Homer1 do not show compensatory changes. Further pharmacological rescue experiments with NMDAR modulators suggest that the behavioral phenotypes related to SCZ and ASD with loss or gain of CYFIP1 function are, at least in part, caused by the abnormal protein synthesis of CYFIP1 targets, including the NMDAR complex. This is the first piece of evidence suggesting that a regulator of protein translation of specific target genes may diametrically contribute to the pathophysiology of both SCZ and ASD.

NMDARs exhibit a critical role in synaptic transmission and plasticity. Human genetic studies revealed that mutations of NMDARs are strongly implicated in the etiology of both SCZ and ASD (68–71). In addition, the expression of NMDARs and their associated complex are frequently altered in human patients with SCZ (72, 73). An imbalance of NMDAR signaling in mouse models results in SCZ and ASD-like phenotypes that can be rescued by pharmacological manipulation of NMDARs (43, 56, 74–76). Therefore, protein expression levels of the NMDAR subunits and their associated complex must be tightly controlled to maintain normal synaptic transmission and behavior. In this study, loss or gain of CYFIP1 function in mouse models led to imbalanced NMDAR signaling with aberrant translational control of CYFIP1 target genes. A subset of the behavioral abnormalities related to SCZ and ASD, such as behavioral despair, impaired social interaction, and exaggerated amphetamine-induced hyperactivity, were restored by balancing the altered NMDAR activities pharmacologically in the adult. However, other behavioral abnormalities including impaired prepulse inhibition in cKO mice and repetitive behavior in cOE mice were not rescued (Figure S6B and data not shown). A recent study suggested that CYFIP1 regulates GABAergic neurotransmission at inhibitory synapses to maintain an excitatory/inhibitory balance (27), implying that these behavoiral abnormalities might be caused by dysregulation of CYFIP1 targets related to GABA receptor signaling, such as *Gabbr2*, *Slc6a1*, and *Slc6a11*. In addition, some behavioral phenotypes might be caused by functions of CYFIP1 in cytoskeleton remodeling (22, 49, 77). Alternatively, CYFIP1 may regulate neuronal developmental processes that are not restored by the later pharmacological treatments used in this study. It remains to be investigated whether other psychotic drug treatments may rescue some of the behavioral phenotypes in these mouse models.

Although it is not straightforward to directly correlate mouse behavioral phenotypes with patient symptoms, our study provides systematic *in vivo* evidence on how abnormal levels of CYFIP1 lead to common and distinct defects associated with SCZ and ASD at the biochemical, synaptic and behavioral levels. Future research on other CNV risk factors for various psychiatric disorders will further highlight the homeostatic control of molecular processes governing synaptic function and behavior.

Supplementary Material

Refer to Web version on PubMed Central for supplementary material.

ACKNOWLEDGEMENTS

We thank members of the Ming and Song laboratories for discussion; L. Liu, Y. Cai, D.G. Johnson, B. Temsamrit and E. LaNoce for technical support, J. Schnoll for lab coordination, and G. Krauss and D.W. Nauen for human surgical cortical tissue. This work was supported by the National Institutes of Health (U19MH106434 and R35NS116843 to H.S., R35NS097370 to G-l.M., R35NS097966 and DA044123 to P.W., and P50DA044123 to V.L.D. and T.M.D.), and Simons Foundation (#308988 to H.S.). T.M.D. is the Leonard and Madlyn Abramson Professor in Neurodegenerative Disease.

REFERENCES

1. Geschwind DH (2009): Advances in Autism. Annual Review of Medicine. 60:367–380.
2. Weinberger DR (1987): Implications of Normal Brain Development for the Pathogenesis of Schizophrenia. Archives of general psychiatry. 44:660–669. [PubMed: 3606332]
3. Malhotra D, Sebat J (2012): CNVs: Harbingers of a Rare Variant Revolution in Psychiatric Genetics. Cell. 148:1223–1241. [PubMed: 22424231]
4. Carroll LS, Owen MJ (2009): Genetic overlap between autism, schizophrenia and bipolar disorder. Genome Med. 1:102. [PubMed: 19886976]
5. Crespi B, Stead P, Elliot M (2010): Comparative genomics of autism and schizophrenia. Proceedings of the National Academy of Sciences. 107:1736–1741.
6. Kenny EM, Cormican P, Furlong S, Heron E, Kenny G, Fahey C, et al. (2014): Excess of rare novel loss-of-function variants in synaptic genes in schizophrenia and autism spectrum disorders. Molecular Psychiatry. 19:872–879. [PubMed: 24126926]
7. Kushima I, Aleksic B, Nakatochi M, Shimamura T, Okada T, Uno Y, et al. (2018): Comparative Analyses of Copy-Number Variation in Autism Spectrum Disorder and Schizophrenia Reveal Etiological Overlap and Biological Insights. Cell Rep. 24:2838–2856. [PubMed: 30208311]
8. Ramocki MB, Zoghbi HY (2008): Failure of neuronal homeostasis results in common neuropsychiatric phenotypes. Nature. 455:912–918. [PubMed: 18923513]
9. Cox D, Butler M (2015): The 15q11.2 BP1–BP2 Microdeletion Syndrome: A Review. International Journal of Molecular Sciences. 16:4068–4082. [PubMed: 25689425]
10. Grozeva D, Conrad DF, Barnes CP, Hurles M, Owen MJ, O'Donovan MC, et al. (2012): Independent estimation of the frequency of rare CNVs in the UK population confirms their role in schizophrenia. Schizophrenia research. 135:1–7. [PubMed: 22130109]
11. Grayton HM, Fernandes C, Rujescu D, Collier DA (2012): Copy number variations in neurodevelopmental disorders. Progress in neurobiology. 99:81–91. [PubMed: 22813947]
12. Vanlerberghe C, Petit F, Malan V, Vincent-Delorme C, Bouquillon S, Boute O, et al. (2015): 15q11.2 microdeletion (BP1–BP2) and developmental delay, behaviour issues, epilepsy and congenital heart disease: A series of 52 patients. European journal of medical genetics. 58:140–147. [PubMed: 25596525]
13. Nishimura Y, Martin CL, Vazquez-Lopez A, Spence SJ, Alvarez-Retuerto AI, Sigman M, et al. (2007): Genome-wide expression profiling of lymphoblastoid cell lines distinguishes different forms of autism and reveals shared pathways. Human molecular genetics. 16:1682–1698. [PubMed: 17519220]
14. van der Zwaag B, Staal WG, Hochstenbach R, Poot M, Spierenburg HA, de Jonge MV, et al. (2009): A co-segregating microduplication of chromosome 15q11.2 pinpoints two risk genes for autism spectrum disorder. American Journal of Medical Genetics Part C: Seminars in Medical Genetics. 9999B:960–966.
15. Stefansson H, Rujescu D, Cichon S, Pietiläinen OPH, Ingason A, Steinberg S, et al. (2008): Large recurrent microdeletions associated with schizophrenia. Nature. 455:232–236. [PubMed: 18668039]

16. Stefansson H, Meyer-Lindenberg A, Steinberg S, Magnusdottir B, Morgen K, Arnarsdottir S, et al. (2013): CNVs conferring risk of autism or schizophrenia affect cognition in controls. Nature. 505:361–366. [PubMed: 24352232]
17. Woo YJ, Kanellopoulos AK, Hemati P, Kirschen J, Nebel RA, Wang T, et al. (2019): Domain-Specific Cognitive Impairments in Humans and Flies With Reduced CYFIP1 Dosage. Biol Psychiatry. 86:306–314. [PubMed: 31202490]
18. Silva AI, G. K, Kendall KM, Bracher-Smith M, Wilkinson LS, Hall J, et al. (2021): Analysis of diffusion tensor imaging data from the UK Biobank confirms dosage effect of 15q11.2 copy-number variation on white matter and shows association with cognition. Biological Psychiatry
19. Silva AI, Ulfarsson MO, Stefansson H, Gustafsson O, Walters GB, Linden DEJ, et al. (2019): Reciprocal White Matter Changes Associated With Copy Number Variation at 15q11.2 BP1-BP2: A Diffusion Tensor Imaging Study. Biol Psychiatry. 85:563–572. [PubMed: 30583851]
20. Writing Committee for the E-CNVWG, van der Meer D, Sonderby IE, Kaufmann T, Walters GB, Abdellaoui A, et al. (2020): Association of Copy Number Variation of the 15q11.2 BP1-BP2 Region With Cortical and Subcortical Morphology and Cognition. JAMA Psychiatry. 77:420–430. [PubMed: 31665216]
21. Napoli I, Mercaldo V, Boyl P, Eleuteri B, Zalfa F, De Rubeis S, et al. (2008): The fragile X syndrome protein represses activity-dependent translation through CYFIP1, a new 4E-BP. Cell. 134:1042–1054. [PubMed: 18805096]
22. De Rubeis S, Pasciuto E, Li KW, Fernández E, Di Marino D, Buzzi A, et al. (2013): CYFIP1 Coordinates mRNA Translation and Cytoskeleton Remodeling to Ensure Proper Dendritic Spine Formation. Neuron. 79:1169–1182. [PubMed: 24050404]
23. Pathania M, Davenport EC, Muir J, Sheehan DF, López-Doménech G, Kittler JT (2014): The autism and schizophrenia associated gene CYFIP1 is critical for the maintenance of dendritic complexity and the stabilization of mature spines. Translational Psychiatry. 4:e374–311. [PubMed: 24667445]
24. Oguro-Ando A, Rosensweig C, Herman E, Nishimura Y, Werling D, Bill BR, et al. (2014): Increased CYFIP1 dosage alters cellular and dendritic morphology and dysregulates mTOR. Molecular Psychiatry. 20:1069–1078. [PubMed: 25311365]
25. Bachmann SO, Sledziowska M, Cross E, Kalbassi S, Waldron S, Chen F, et al. (2019): Behavioral training rescues motor deficits in Cyfip1 haploinsufficiency mouse model of autism spectrum disorders. Transl Psychiatry. 9:29. [PubMed: 30664619]
26. Bozdagi O, Sakurai T, Dorr N, Pilorge M, Takahashi N, Buxbaum JD (2012): Haploinsufficiency of Cyfip1 Produces Fragile X-Like Phenotypes in Mice. PloS one. 7:e42422. [PubMed: 22900020]
27. Davenport EC, Szulc BR, Drew J, Taylor J, Morgan T, Higgs NF, et al. (2019): Autism and Schizophrenia-Associated CYFIP1 Regulates the Balance of Synaptic Excitation and Inhibition. Cell Rep. 26:2037–2051 e2036. [PubMed: 30784587]
28. Dominguez-Iturza N, Lo AC, Shah D, Armendariz M, Vannelli A, Mercaldo V, et al. (2019): The autism- and schizophrenia-associated protein CYFIP1 regulates bilateral brain connectivity and behaviour. Nature communications. 10:3454.
29. Silva AI, Haddon JE, Ahmed Syed Y, Trent S, Lin TE, Patel Y, et al. (2019): Cyfip1 haploinsufficient rats show white matter changes, myelin thinning, abnormal oligodendrocytes and behavioural inflexibility. Nature communications. 10:3455.
30. Fricano-Kugler C, Gordon A, Shin G, Gao K, Nguyen J, Berg J, et al. (2019): CYFIP1 overexpression increases fear response in mice but does not affect social or repetitive behavioral phenotypes. Molecular autism. 10:25. [PubMed: 31198525]
31. Babbs RK, Beierle JA, Ruan QT, Kelliher JC, Chen MM, Feng AX, et al. (2019): Cyfip1 Haploinsufficiency Increases Compulsive-Like Behavior and Modulates Palatable Food Intake in Mice: Dependence on Cyfip2 Genetic Background, Parent-of Origin, and Sex. G3 (Bethesda). 9:3009–3022. [PubMed: 31324746]
32. Chung L, Wang X, Zhu L, Towers AJ, Cao X, Kim IH, et al. (2015): Parental origin impairment of synaptic functions and behaviors in cytoplasmic FMRP interacting protein 1 (Cyfip1) deficient mice. Brain Res. 1629:340–350. [PubMed: 26474913]

33. Zhao Q, Li T, Zhao X, Huang K, Wang T, Li Z, et al. (2013): Rare CNVs and Tag SNPs at 15q11.2 Are Associated With Schizophrenia in the Han Chinese Population. Schizophrenia bulletin. 39:712–719. [PubMed: 22317777]
34. Waltes R, Duketis E, Knapp M, Anney RJL, Huguet G, Schlitt S, et al. (2014): Common variants in genes of the postsynaptic FMRP signalling pathway are risk factors for autism spectrum disorders. Human Genetics. 133:781–792. [PubMed: 24442360]
35. Noroozi R, Omrani MD, Sayad A, Taheri M, Ghafouri-Fard S (2018): Cytoplasmic FMRP interacting protein 1/2 (CYFIP1/2) expression analysis in autism. Metab Brain Dis. 33:1353–1358. [PubMed: 29752658]
36. Wang J, Tao Y, Song F, Sun Y, Ott J, Saffen D (2015): Common Regulatory Variants of CYFIP1Contribute to Susceptibility for Autism Spectrum Disorder (ASD) and Classical Autism. Annals of human genetics. 79:329–340. [PubMed: 26094621]
37. Silverman JL, Yang M, Lord C, Crawley JN (2010): Behavioural phenotyping assays for mouse models of autism. Nat Rev Neurosci. 11:490–502. [PubMed: 20559336]
38. van den Buuse M (2010): Modeling the positive symptoms of schizophrenia in genetically modified mice: pharmacology and methodology aspects. Schizophrenia bulletin. 36:246–270. [PubMed: 19900963]
39. Rapin I, Tuchman RF (2008): Autism: Definition, Neurobiology, Screening, Diagnosis. Pediatric Clinics of North America. 55:1129–1146. [PubMed: 18929056]
40. Deacon RMJ (2006): Digging and marble burying in mice: simple methods for in vivo identification of biological impacts. Nature Protocols. 1:122–124. [PubMed: 17406223]
41. Sadakata T, Washida M, Iwayama Y, Shoji S, Sato Y, Ohkura T, et al. (2007): Autistic-like phenotypes in Cadps2-knockout mice and aberrant CADPS2 splicing in autistic patients. Journal of Clinical Investigation. 117:931–943. [PubMed: 17380209]
42. Satoh Y, Endo S, Nakata T, Kobayashi Y, Yamada K, Ikeda T, et al. (2011): ERK2 contributes to the control of social behaviors in mice. Journal of Neuroscience. 31:11953–11967. [PubMed: 21849556]
43. Won H, Lee H-R, Gee HY, Mah W, Kim J-I, Lee J, et al. (2012): Autistic-like social behaviour in Shank2-mutant mice improved by restoring NMDA receptor function. Nature. 486:261–265. [PubMed: 22699620]
44. Zhao J, Ohsumi TK, Kung JT, Ogawa Y, Grau DJ, Sarma K, et al. (2010): Genome-wide identification of polycomb-associated RNAs by RIP-seq. Mol Cell. 40:939–953. [PubMed: 21172659]
45. Darnell JC, Van Driesche SJ, Zhang C, Hung KY, Mele A, Fraser CE, et al. (2011): FMRP stalls ribosomal translocation on mRNAs linked to synaptic function and autism. Cell. 146:247–261. [PubMed: 21784246]
46. Panja D, Kenney JW, D'Andrea L, Zalfa F, Vedeler A, Wibrand K, et al. (2014): Two-Stage Translational Control of Dentate Gyrus LTP Consolidation Is Mediated by Sustained BDNF-TrkB Signaling to MNK. Cell Reports. 9:1430–1445. [PubMed: 25453757]
47. Aviner R, Geiger T, Elroy-Stein O (2014): Genome-wide identification and quantification of protein synthesis in cultured cells and whole tissues by puromycin-associated nascent chain proteomics (PUNCH-P). Nature Protocols. 9:751–760. [PubMed: 24603934]
48. Feng W, Zhang M (2009): Organization and dynamics of PDZ-domain-related supramodules in the postsynaptic density. Nature Reviews Neuroscience. 10:87–99. [PubMed: 19153575]
49. Yoon KJ, Nguyen HN, Ursini G, Zhang F, Kim NS, Wen Z, et al. (2014): Modeling a genetic risk for schizophrenia in iPSCs and mice reveals neural stem cell deficits associated with adherens junctions and polarity. Cell Stem Cell. 15:79–91. [PubMed: 24996170]
50. Fromer M, Pocklington AJ, Kavanagh DH, Williams HJ, Dwyer S, Gormley P, et al. (2014): De novo mutations in schizophrenia implicate synaptic networks. Nature. 506:179–184. [PubMed: 24463507]
51. Lakhan SE, Caro M, Hadzimichalis N (2013): NMDA Receptor Activity in Neuropsychiatric Disorders. Frontiers in Psychiatry. 4:52. [PubMed: 23772215]
52. Lee E-J, Choi SY, Kim E (2015): NMDA receptor dysfunction in autism spectrum disorders. Current Opinion in Pharmacology. 20:8–13. [PubMed: 25636159]

53. van den Buuse M, Halley P, Hill R, Labots M, Martin S (2012): Altered N-methyl-d-aspartate receptor function in reelin heterozygous mice: Male–female differences and comparison with dopaminergic activity. Progress in neuro-psychopharmacology & biological psychiatry. 37:237–246. [PubMed: 22361156]
54. Zhou X, Zheng F, Moon C, Schluter OM, Wang H (2012): Bi-directional regulation of CaMKIIalpha phosphorylation at Thr286 by NMDA receptors in cultured cortical neurons. Journal of neurochemistry. 122:295–307. [PubMed: 22582824]
55. Waxman EA, Lynch DR (2005): N-methyl-D-aspartate receptor subtype mediated bidirectional control of p38 mitogen-activated protein kinase. The Journal of biological chemistry. 280:29322–29333. [PubMed: 15967799]
56. Chung W, Choi SY, Lee E, Park H, Kang J, Park H, et al. (2015): Social deficits in IRSp53 mutant mice improved by NMDAR and mGluR5 suppression. Nat Neurosci. 18:435–443. [PubMed: 25622145]
57. Stazi M, Wirths O (2021): Chronic Memantine Treatment Ameliorates Behavioral Deficits, Neuron Loss, and Impaired Neurogenesis in a Model of Alzheimer's Disease. Mol Neurobiol. 58:204–216. [PubMed: 32914393]
58. Lockrow J, Boger H, Bimonte-Nelson H, Granholm AC (2011): Effects of long-term memantine on memory and neuropathology in Ts65Dn mice, a model for Down syndrome. Behav Brain Res. 221:610–622. [PubMed: 20363261]
59. Gao Y, Payne RS, Schurr A, Hougland T, Lord J, Herman L, et al. (2011): Memantine reduces mania-like symptoms in animal models. Psychiatry Res. 188:366–371. [PubMed: 21269711]
60. Blundell J, Blaiss CA, Etherton MR, Espinosa F, Tabuchi K, Walz C, et al. (2010): Neuroligin-1 deletion results in impaired spatial memory and increased repetitive behavior. Journal of Neuroscience. 30:2115–2129. [PubMed: 20147539]
61. Zhou J, Blundell J, Ogawa S, Kwon CH, Zhang W, Sinton C, et al. (2009): Pharmacological inhibition of mTORC1 suppresses anatomical, cellular, and behavioral abnormalities in neural-specific Pten knock-out mice. J Neurosci. 29:1773–1783. [PubMed: 19211884]
62. Young DM, Schenk AK, Yang SB, Jan YN, Jan LY (2010): Altered ultrasonic vocalizations in a tuberous sclerosis mouse model of autism. Proc Natl Acad Sci U S A. 107:11074–11079. [PubMed: 20534473]
63. Tsai PT, Hull C, Chu Y, Greene-Colozzi E, Sadowski AR, Leech JM, et al. (2012): Autistic-like behaviour and cerebellar dysfunction in Purkinje cell Tsc1 mutant mice. Nature. 488:647–651. [PubMed: 22763451]
64. Santini E, Huynh TN, MacAskill AF, Carter AG, Pierre P, Ruggero D, et al. (2012): Exaggerated translation causes synaptic and behavioural aberrations associated with autism. Nature. 493:411–415. [PubMed: 23263185]
65. Gkogkas CG, Khoutorsky A, Ran I, Rampakakis E, Nevarko T, Weatherill DB, et al. (2012): Autism-related deficits via dysregulated eIF4E-dependent translational control. Nature. 493:371–377. [PubMed: 23172145]
66. Topol A, English JA, Flaherty E, Rajarajan P, Hartley BJ, Gupta S, et al. (2015): Increased abundance of translation machinery in stem cell-derived neural progenitor cells from four schizophrenia patients. Transl Psychiatry. 5:e662. [PubMed: 26485546]
67. English JA, Fan Y, Focking M, Lopez LM, Hryniewiecka M, Wynne K, et al. (2015): Reduced protein synthesis in schizophrenia patient-derived olfactory cells. Transl Psychiatry. 5:e663. [PubMed: 26485547]
68. Schizophrenia Working Group of the Psychiatric Genomics C (2014): Biological insights from 108 schizophrenia-associated genetic loci. Nature. 511:421–427. [PubMed: 25056061]
69. O'Roak BJ, Deriziotis P, Lee C, Vives L, Schwartz JJ, Girirajan S, et al. (2011): Exome sequencing in sporadic autism spectrum disorders identifies severe de novo mutations. Nat Genet. 43:585–589. [PubMed: 21572417]
70. De Rubeis S, He X, Goldberg AP, Poultney CS, Samocha K, Cicek AE, et al. (2014): Synaptic, transcriptional and chromatin genes disrupted in autism. Nature. 515:209–215. [PubMed: 25363760]

71. Takasaki Y, Koide T, Wang C, Kimura H, Xing J, Kushima I, et al. (2016): Mutation screening of GRIN2B in schizophrenia and autism spectrum disorder in a Japanese population. Scientific reports. 6:33311. [PubMed: 27616045]

72. Li W, Ghose S, Gleason K, Begovic A, Perez J, Bartko J, et al. (2015): Synaptic proteins in the hippocampus indicative of increased neuronal activity in CA3 in schizophrenia. Am J Psychiatry. 172:373–382. [PubMed: 25585032]

73. Akbarian S, Sucher NJ, Bradley D, Tafazzoli A, Trinh D, Hetrick WP, et al. (1996): Selective alterations in gene expression for NMDA receptor subunits in prefrontal cortex of schizophrenics. J Neurosci. 16:19–30. [PubMed: 8613785]

74. Mohn AR, Gainetdinov RR, Caron MG, Koller BH (1999): Mice with reduced NMDA receptor expression display behaviors related to schizophrenia. Cell. 98:427–436. [PubMed: 10481908]

75. Belforte JE, Zsiros V, Sklar ER, Jiang Z, Yu G, Li Y, et al. (2010): Postnatal NMDA receptor ablation in corticolimbic interneurons confers schizophrenia-like phenotypes. Nat Neurosci. 13:76–83. [PubMed: 19915563]

76. Gandal MJ, Anderson RL, Billingslea EN, Carlson GC, Roberts TPL, Siegel SJ (2012): Mice with reduced NMDA receptor expression: more consistent with autism than schizophrenia? Genes, brain, and behavior. 11:740–750. [PubMed: 22726567]

77. Santini E, Huynh TN, Longo F, Koo SY, Mojica E, D'Andrea L, et al. (2017): Reducing eIF4E-eIF4G interactions restores the balance between protein synthesis and actin dynamics in fragile X syndrome model mice. Sci Signal. 10:eaan0665. [PubMed: 29114037]

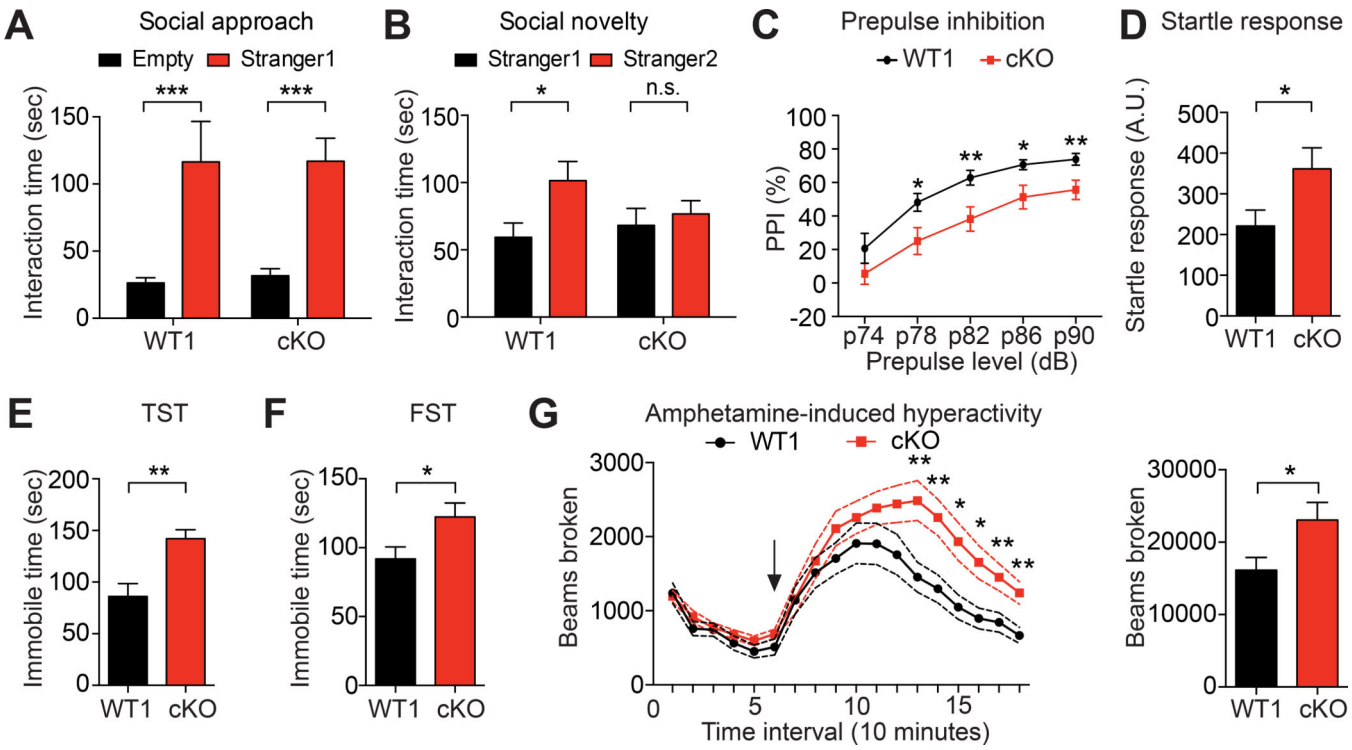

Figure 1. *Cyfip1* cKO mice displayed impaired social novelty recognition, abnormal sensorimotor gating, elevated despair and altered psychostimulant response.

(A-B) Normal social approach and impaired social novelty recognition of cKO mice in the three-chamber assay. In the first stage, both WT1 mice and cKO mice showed a significant preference for a mouse (stranger 1) over an empty cage, as measured by time spent in close interaction (**A**). In the second stage, cKO mice showed no preference for a novel mouse (stranger 2) over a familiar mouse (stranger 1), while WT1 mice interacted significantly more with stranger 2 than stranger 1 (**B**). Values represent mean ± SEM (n = 10 WT1, 10 cKO; ***p < 0.001; * p < 0.05; n.s.: p > 0.05; Student's t-test). **(C-D)** Abnormal prepulse inhibition (**C**) and increased basal acoustic startle response (120 dB, **D**) of cKO mice compared with WT1 mice. Values represent mean ± SEM (n = 19 WT1, 15 cKO; *p < 0.05; **p < 0.01; Student's t-test). **(E-F)** Elevated behavioral despair in cKO mice. The immobile time in both tail suspension test (TST, **E**) and forced swim test (FST, **F**) was increased in cKO mice compared with WT1 mice. Values represent mean ± SEM (n = 19 WT1, 15 cKO; *p < 0.05; **p < 0.01; Student's t-test). **(G)** Enhanced amphetamine-induced hyperactivity in cKO mice compared with WT1 mice. Amphetamine (2.5 mg/kg, i.p.) was injected after 1 hr habituation in an open field. Shown on the left is the trace of the locomotor activity presented as the number of beams broken every 10 min. An arrow represents the time of the amphetamine injection. Shown on the right is the total number of beams broken after amphetamine injection. Values represent mean ± SEM (n = 11 WT1, 14 cKO; **p < 0.01; *p < 0.05; n.s.: p > 0.05; Student's t test).

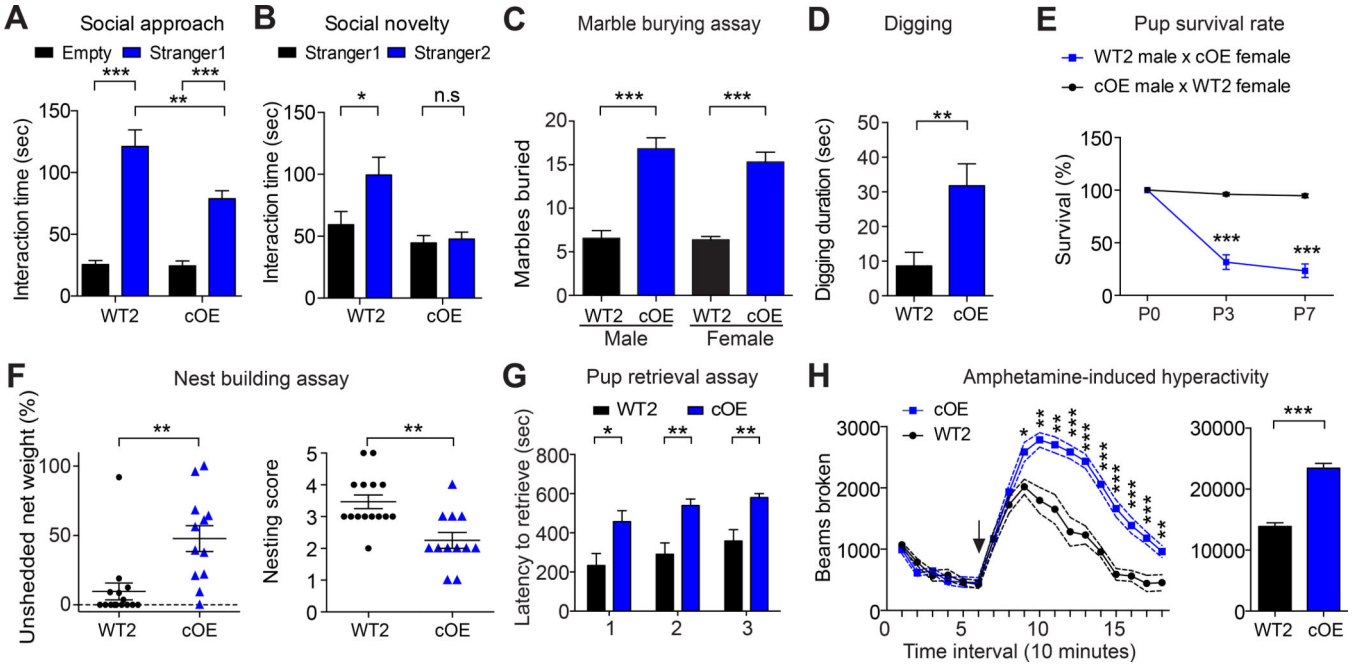

Figure 2. *Cyfip1* cOE mice displayed impaired social interaction, increased repetitive behaviors, abnormal maternal behaviors and altered psychostimulant response.

(A-B) Reduced social approach and impaired social novelty recognition of cOE mice in the three-chamber assay. In the first stage, cOE mice showed a significantly lower preference for a mouse (stranger 1) over an empty cage compared with WT2 mice (**A**). In the second stage, cOE mice showed no preference for a novel mouse (stranger 2) over a familiar mouse (stranger 1), while WT2 mice interacted significantly more with stranger 2 than stranger 1 (**B**). Values represent mean ± SEM (n = 13 WT2, 13 cOE; ***p < 0.001; **p < 0.01; *p < 0.05; n.s.: p > 0.05; One-way ANOVA). **(C)** Increased repetitive behavior of cOE mice in the marble burying test. Number of marbles buried during a 30 min test period was counted. Values represent mean ± SEM (n = 16 WT2/male, 11 cOE/male, 8 WT2/female, 13 cOE/female; ***p < 0.001; Student's t-test). **(D)** Increased digging behavior of cOE mice. Time spent in digging was measured during a 10 min test period. Values represent mean ± SEM (n = 11 WT2, 10 cOE; **p < 0.01; Student's t-test). **(E)** Pups from cOE dams showed reduced survival rate in the early postnatal period. Survival rate of pups from each litter was quantified according to genotypes of the dams. Values represent mean ± SD (n = 10 WT2, 14 cOE litters; ***p < 0.001; Student's t-test). **(F)** cOE females displayed abnormal nest building behavior. Shown on the left is the percentage weight of the un-shredded nest and shown on the right is the nest building score 24 h after a new nestlet presentation. Values represent mean ± SEM (n = 15 WT2, 12 cOE; **p < 0.01; Student's t-test). **(G)** cOE females showed impaired pup retrieval behavior. The retrieval latencies of three pups in the pup retrieval test are shown. Values represent mean ± SEM (n = 13 WT2, 11 cOE; **p < 0.01; *p < 0.05; Student's t test). **(H)** Enhanced amphetamine-induced hyperactivity in cOE mice compared with WT2 mice. Shown on the left is the trace of the locomotor activity presented as the number of beams broken every 10 min. An arrow represents the time of the amphetamine injection. Shown on the right is the total number of beams broken after the

amphetamine injection. Values represent mean ± SEM (n = 11 WT1, 14 cKO; ***p < 0.001; **p < 0.01; *p < 0.05; Student's t-test).

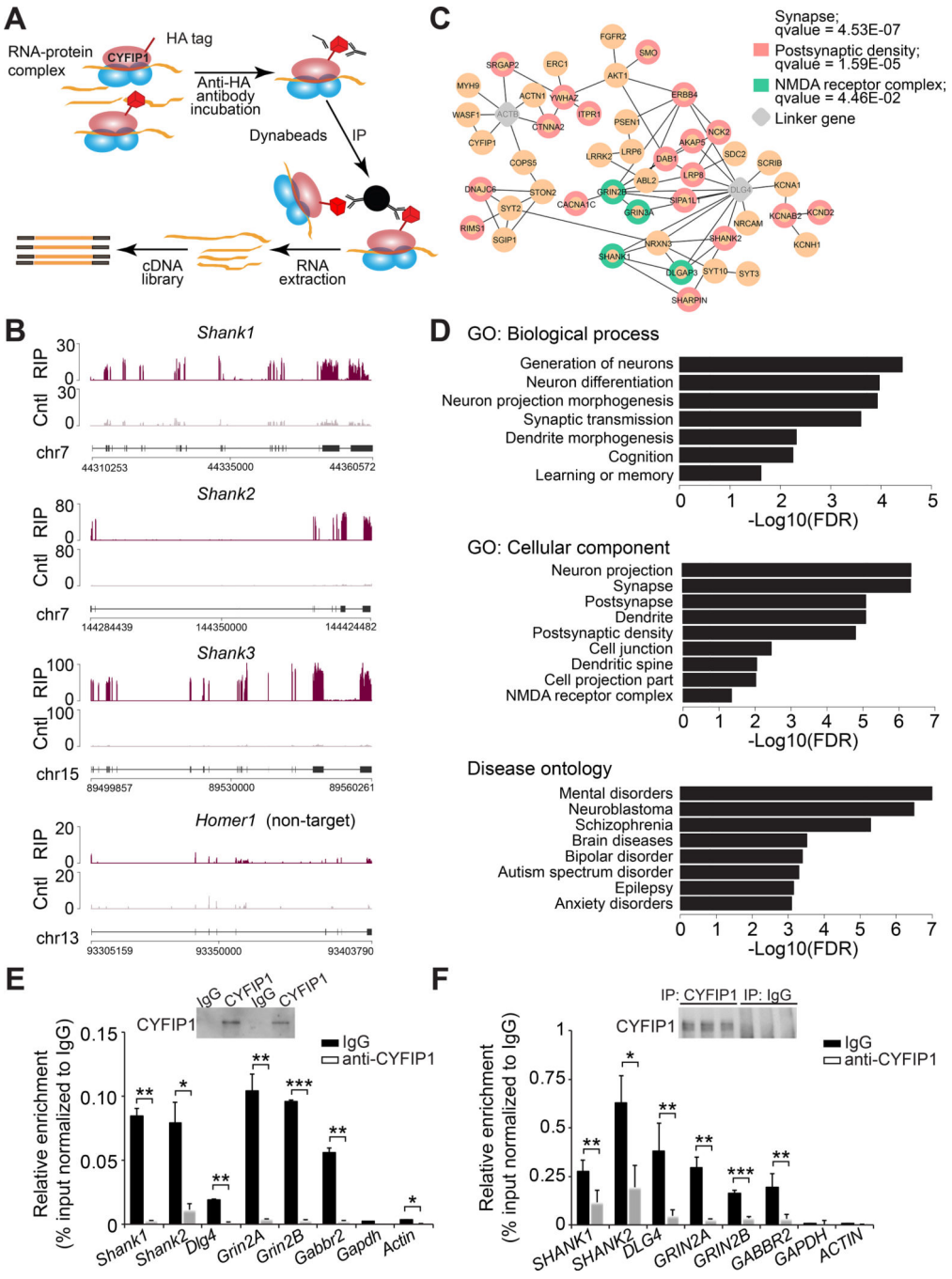

Figure 3. RIP-seq experiments reveal mRNA targets of CYFIP1.

(A) An experimental scheme for RIP-seq. **(B)** Protein-protein interaction network showing interactions between mRNA targets of CYFIP1 related to synapse, postsynaptic density and NMDAR complex. q-values: p-value adjusted for false discovery rate (FDR) using Benjamini-Hochberg procedure. **(C)** Representative coverage plots for mRNA targets of CYFIP1 (*Shank1*, *Shank2*, *Shank3*). Coverage plot for Homer1 (control, non-target) is also shown for comparison. Read coverage is normalized by library size. Top panel shows coverage in the RIP library; middle panel shows the control library, and lower panel shows

a representation of the genetic features of each mRNA. For genes with multiple transcripts, the longest one is shown. **(D)** GO analysis of CYFIP1 mRNA targets reveals enrichment for terms related to neuronal function and postsynaptic density. Disease ontology analysis shows enrichment for genes associated with mental disorders, including schizophrenia and ASD. **(E)** Association of the CYFIP1 protein with mRNAs encoding the NMDAR complex. Shown on the top is a representative immunoblot of the CYFIP1 protein pulled-down by immunoprecipitation (IP) from hippocampal lysates. Shown on the bottom are quantitative PCR results from co-IPed mRNAs by anti-CYFIP1 antibody compared with co-IPed mRNAs by control IgG. Values represent mean ± SEM (n = 4 independent experiments; ***p < 0.001; **p < 0.01; *p < 0.05; Student's t-test). **(F)** RIP-qPCR of human surgical cerebral cortex samples confirms that CYFIP1 binds its targets in the human brain. Values represent mean ± SEM (n = 3 independent experiments; ***p < 0.001; **p < 0.01; *p < 0.05; Student's t-test).

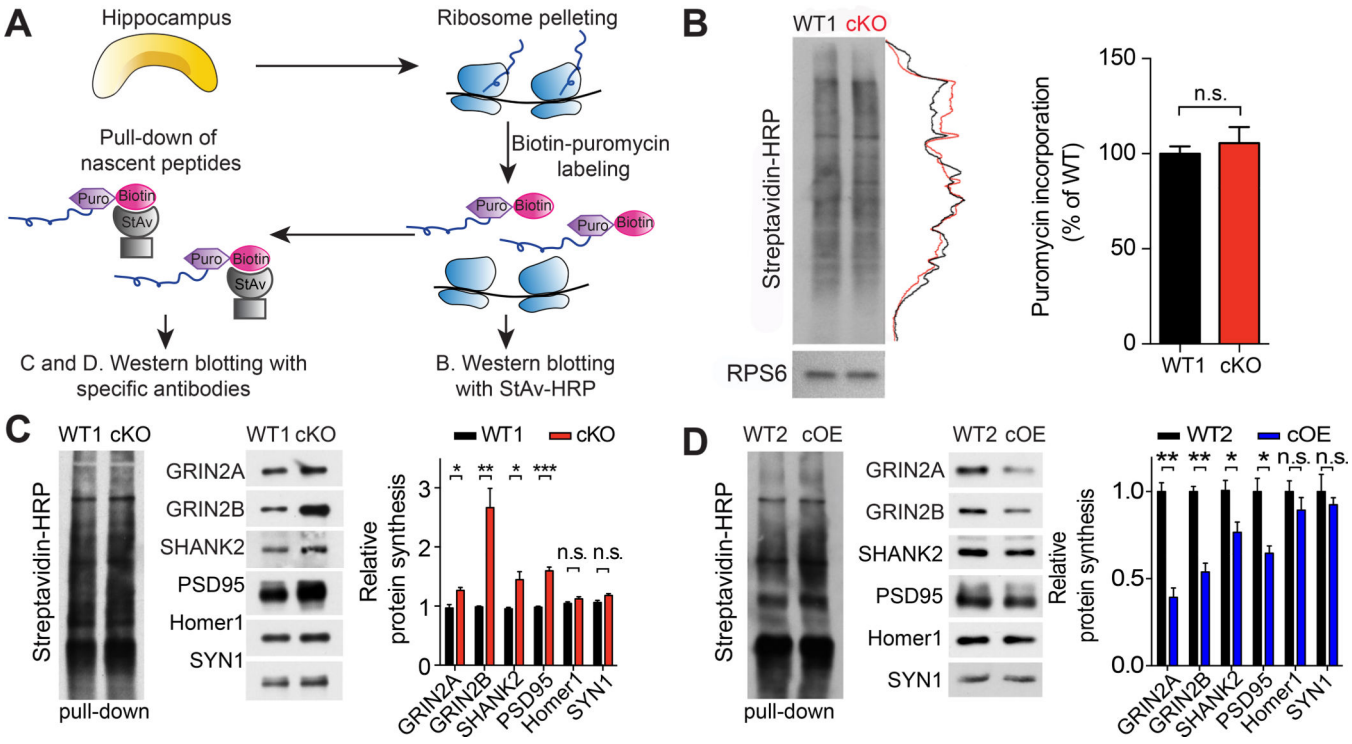

Figure 4. Translational regulation of mRNAs encoding the NMDAR complex by CYFIP1.

(A) A schematic diagram of the experimental design. Ribosomal fractions from hippocampal lysates were pelleted by ultracentrifugation, and then labeled with biotin-puromycin to release newly synthesizing peptides. Released biotin-puromycin-tagged nascent peptides were directly applied to Western blotting with HRP-conjugated streptavidin (StAv-HRP) to monitor the general translation rate (**B**), or pulled-down with magnetic beads conjugated with streptavidin and applied to Western blotting with specific antibodies (**C-D**). **(B)** Normal general translation rate in cKO mice. Shown on the left is a representative immunoblot of total biotin-puromycin labeled peptide detected by StAV-HRP. Vertical line traces of the HRP signal on each lane are shown on the right of the immunoblot. HRP signals were normalized with RPS6 signals and quantified. Values represent mean ± SEM (n = 3 independent experiments, 3 animals per group in each experiment; n.s.: $p > 0.05$; Student's t-test). **(C-D)** Protein synthesis for the NMDAR complex was increased in cKO mice (**C**) and reduced in the cOE mice (**D**). Shown on the left are representative immunoblots of the total pulled-down nascent peptides detected by StAV-HRP. The same samples were applied to Western blotting with specific antibodies shown in the middle. Relative protein synthesis in cKO and cOE mice were normalized by StAV-HRP signals, quantified and compared with WT1 and WT2 mice, respectively, shown on the right. Values represent mean ± SEM (n = 3 independent experiments, 3 animals per group in each experiment; ***$p < 0.001$, **$p < 0.01$; *$p < 0.05$; n.s.: $p > 0.05$; Student's t-test).

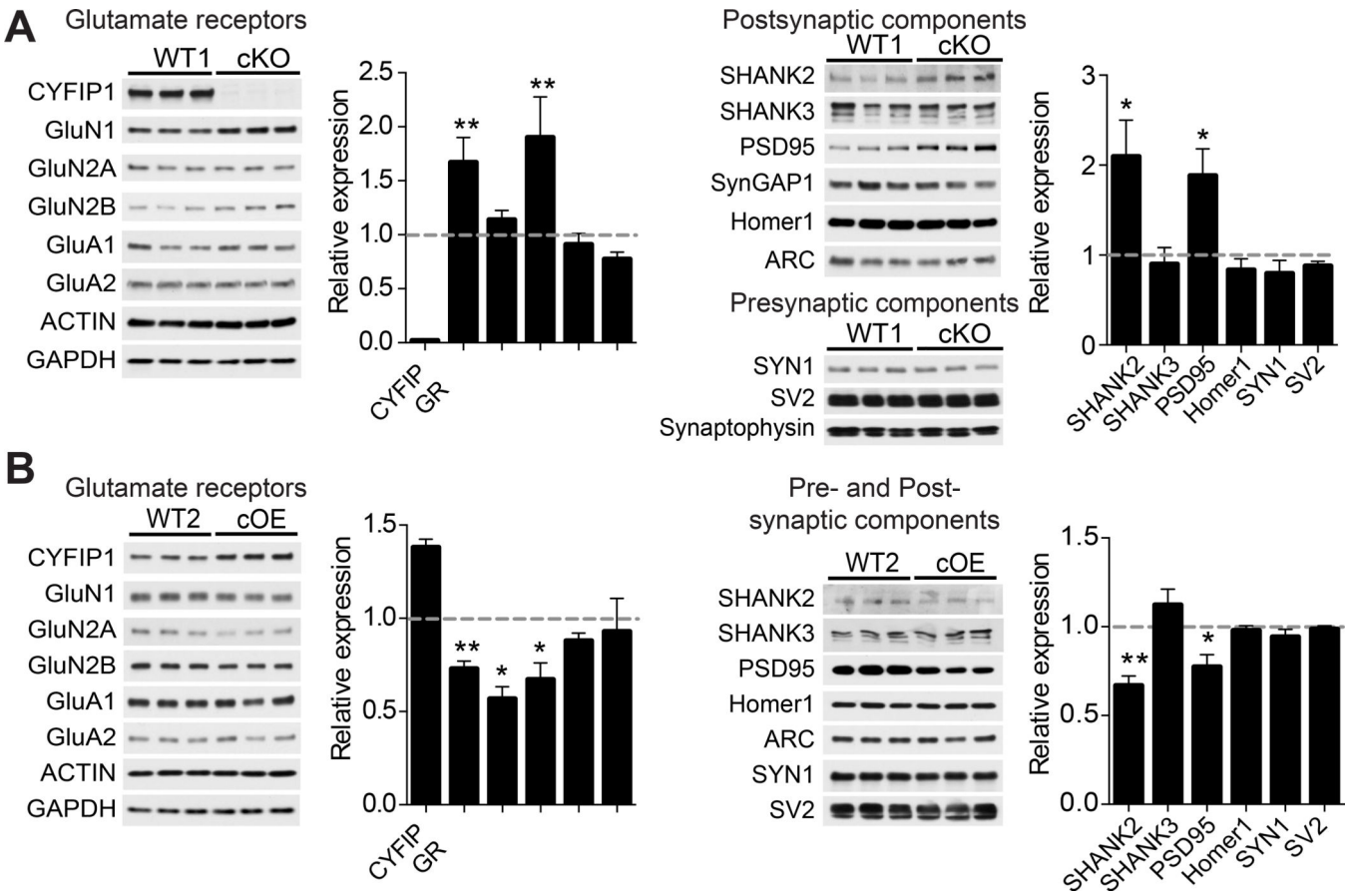

Figure 5. Altered postsynaptic protein expression in synapses with differential *Cyfip1* dosages.

(A) Increased expression of the NMDAR subunits and associated complex in cKO mice. Shown are representative immunoblots of synaptosomal fractions from the hippocampal lysates of 3-month-old littermate WT1 and cKO mice. All data were normalized to ACTIN levels for the loading control, and then the protein expression levels of cKO mice were normalized to that of WT1 mice and plotted as relative changes of the expression level. Values represent mean ± SEM (n = 3–7 animals; **p < 0.01; *p < 0.05; Student's t-test). **(B)** Decreased expression of the NMDAR subunits and associated complex in cKO mice. Shown are representative immunoblots of synaptosomal fractions from the hippocampal lysates of 3-month-old littermate WT2 and cOE mice. All data were normalized to ACTIN levels for the loading control, and then the protein expression levels of cOE mice were normalized to that of WT2 mice and plotted as relative changes of the expression level. Values represent mean ± SEM (n = 3–6 animals; **p < 0.01; *p < 0.05; Student's t-test).

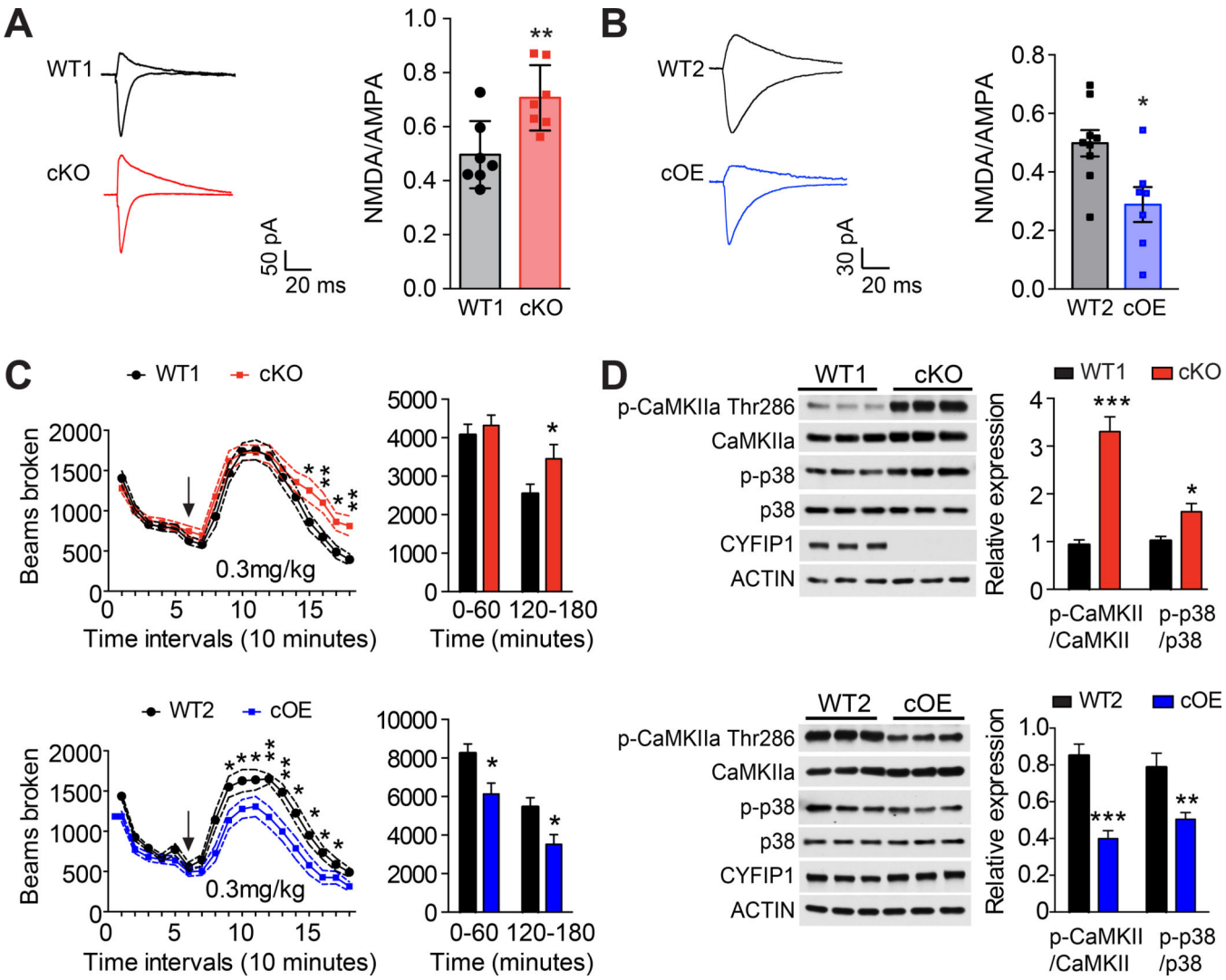

Figure 6. Reciprocal changes in NMDAR function in the *Cyfip1* cKO and cOE mice.

(A-B) NMDA/AMPA ratio recorded from acute hippocampal slices of cKO and cOE mice. Shown on the left are sample recording traces. Shown on the right are summary of NMDA/AMPA mediated evoked synaptic current ratio. Values represent mean ± SEM (n = 7 WT1, 7 cKO, 9 WT2, 7 cOE; **p < 0.01; *p < 0.05; Student's t-test). **(C)** Reciprocal sensitivity on MK-801 administration in cKO (upper panel) and cOE (lower panel) mice. Shown on the left, MK-801 (0.3 mg/kg, i.p.) was injected after a 1 hr habituation, and the locomotor activity in an open field was presented by the number of beams broken every 10 min. Arrows represent the time of the MK-801 injection. Shown on the right, locomotor activity was quantified during the first 1 hr and the last 1 hr after MK-801 injection. Values represent mean ± SEM (n = 15 WT1, 14 cKO, 9 WT2, 12 cOE; **p < 0.01; *p < 0.05; Student's t-test). **(D)** Reciprocal alteration in NMDAR-mediated signaling in cKO and cOE mice. Shown on the left are representative immunoblots of the synaptosomal fraction from the hippocampal lysate of 3-month-old mice. Levels of phosphorylated CaMKIIα and p38 were increased in cKO mice compared with WT1 mice, but decreased in cOE mice compared with WT2 mice. Shown on the right are quantified levels of phosphorylated

protein normalized to the amount of total protein. Values represent mean ± SEM (n = 6 animals; ***p < 0.001; **p < 0.01; *p < 0.05; Student's t test).

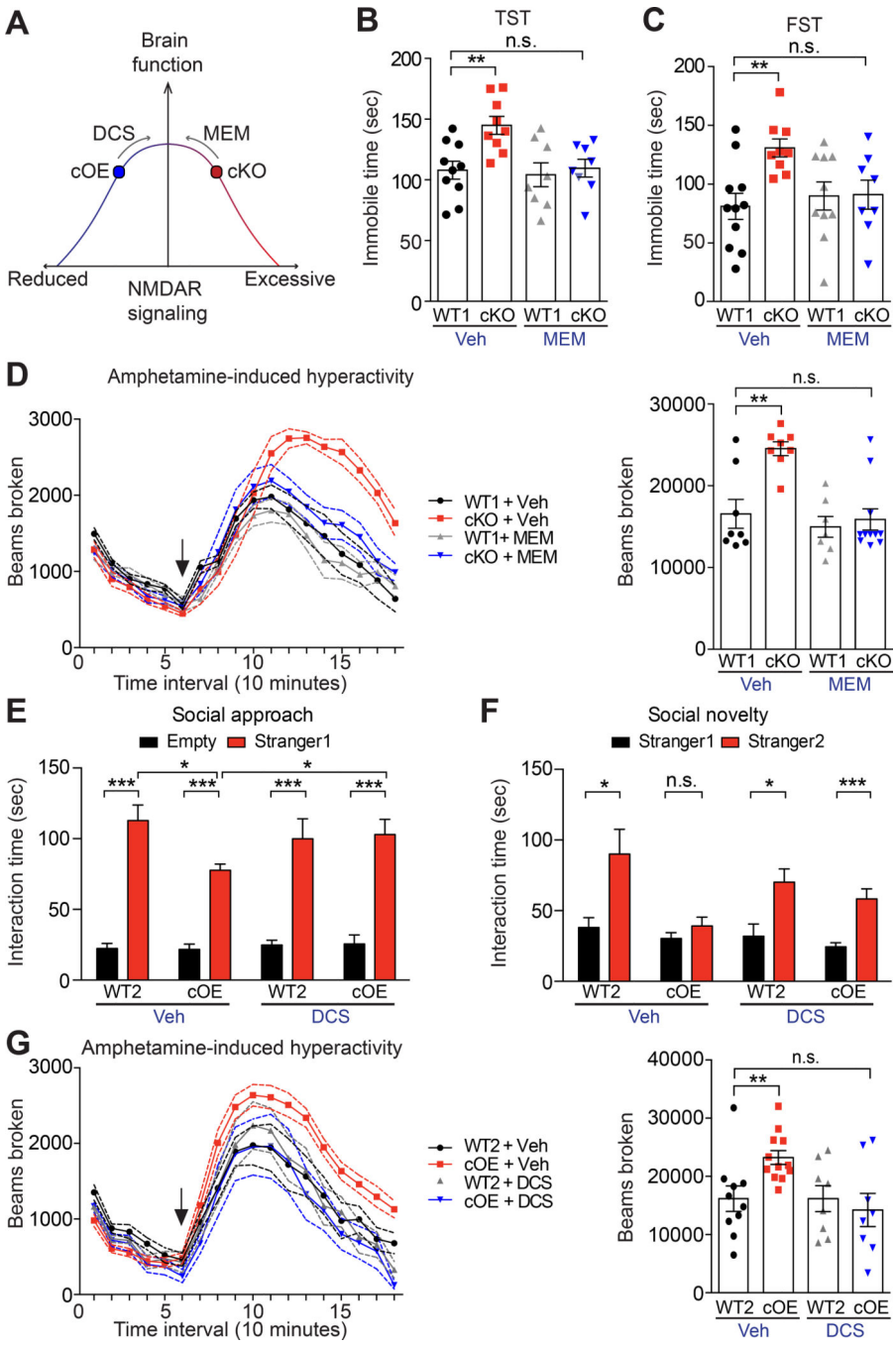

Figure 7. Treatment with memantine in cKO and D-cycloserin in cOE rescued behavioral abnormalities.

(A) A model of NMDAR dysfunction with different levels of *Cyfip1* and pharmacological approaches to re-balance NMDAR signaling. **(B-C)** Behavioral despair in cKO mice was rescued by memantine (MEM), but not vehicle (VEH) treatment. Immobile time in both the TST (**B**) and FST (**C**) was restored in cKO mice after memantine treatment to the level of WT1 mice. Values represent mean ± SEM (TST: n = 10 WT1+VEH, 9 cKO+VEH, 8 WT1+MEM, 8 cKO+MEM; FST: n = 11 WT1+VEH, 9 cKO+VEH, 10 WT1+MEM, 8

cKO+MEM; **p < 0.01; n.s: p > 0.05; One-way ANOVA). **(D)** The level of amphetamine-induced hyperactivity in cKO mice was restored to the level of WT1 mice after memantine treatment. Shown on the left is the trace of locomotor activity. An arrow represents the time of amphetamine injection. Shown on the right is the total number of beams broken after the amphetamine injection. Values represent mean ± SEM. (n = 8 WT1+VEH, 8 cKO+VEH, 7 WT1+MEM, 11 cKO+MEM; **p < 0.01; n.s: p > 0.05; Student's t-test). **(E-F)** Social impairments of cOE mice were improved after D-cycloserin (DCS) treatment. In the first stage, interaction time with stranger 1 by cOE mice after DCS treatment was significantly increased compared to cOE mice without treatment, similar to WT1 mice with or without treatment (**E**). In the second stage, cOE mice showed a significant preference for stranger 2 after DCS treatment, whereas the non-treated cOE mice showed no preference for stranger 2 (**F**). Values represent mean ± SEM (n = 7 WT2+VEH, 7 cOE+VEH, 7 WT2+DCS, 7 cOE+DCS; ***p < 0.001; *p < 0.05; n.s: p > 0.05; One-way ANOVA). **(G)** The level of amphetamine-induced hyperactivity in cOE mice was restored to the level of WT2 mice after DCS treatment. Shown on the left is the trace of locomotor activity. An arrow represents the time of amphetamine injection. Shown on the right is the total number of beams broken after the amphetamine injection. Values represent mean ± SEM (n = 10 WT2+VEH, 12 cOE+VEH, 8 WT2+DCS, 8 cOE+DCS; **p < 0.01; n.s.: p > 0.05; One-way ANOVA).

Key Resource table

Resource Type	Specific Reagent or Resource	Source or Reference	Identifiers	Additional Information
Add additional rows as needed for each resource type	Include species and sex when applicable.	Include name of manufacturer, company, repository, individual, or research lab. Include PMID or DOI for references; use “this paper” if new.	Include catalog numbers, stock numbers, database IDs or accession numbers, and/or RRIDs. RRIDs are highly encouraged; search for RRIDs at https://scicrunch.org/resources.	Include any additional information or notes if necessary.
Antibody	Mouse anti-ACTIN	Millipore	MAB1501, RRID:AB_2223041	1/5000 dilution
Antibody	Rabbit anti-ACTIN	Cytoskeleton	AAN01, RRID:AB_10708070	1/2000 dilution
Antibody	Rabbit anti-ARC	Synaptic Systems	156003, RRID:AB_887694	1/3000 dilution
Antibody	Mouse anti-bIII-Tubulin	Sigma Aldrich	T5201, RRID:AB_609915	1/3000 dilution
Antibody	Mouse anti-CaMKIIa	Santa Cruz Biotech	sc-13141, RRID:AB_626789	1/3000 dilution
Antibody	Rabbit anti-CYFIP1	Millipore	AB6046, RRID:AB_10807712	1/3000 dilution
Antibody	Mouse anti-GAPDH	Abcam	AB9484, RRID:AB_307274	1/5000 dilution
Antibody	Rabbit anti-GRIA1	Alomone Labs	AGC-004, RRID:AB_2039878	1/2000 dilution
Antibody	Mouse anti-GRIA2	Millipore	MAB397, RRID:AB_2113875	1/2000 dilution
Antibody	Mouse anti-GRIN1	Millipore	MAB363, RRID:AB_94946	1/2000 dilution
Antibody	Rabbit anti-GRIN2A	Millipore	05–901R, RRID:AB_11215116	1/2000 dilution
Antibody	Rabbit anti-GRIN2B	Abcam	PRB-512P, RRID:AB_10720558	1/2000 dilution
Antibody	Mouse anti-HA	Covance	MMS-101P, RRID:AB_2314672	1/2000 dilution
Antibody	Mouse anti-HOMER1	Synaptic Systems	160011, RRID:AB_2120992	1/3000 dilution
Antibody	Mouse anti-p38 MAPK	Cell signaling	9228, RRID:AB_10694990	1/1000 dilution
Antibody	Rabbit anti-phospho-p38 MAPK	Cell signaling	9215, RRID:AB_331762	1/1000 dilution
Antibody	Rabbit anti-phospho-CaMKIIa	Cell signaling	3361, RRID:AB_2275070	1/1000 dilution
Antibody	Mouse anti-PSD95	Synaptic Systems	124011, RRID:AB_10804286	1/3000 dilution
Antibody	Mouse anti-SHANK2	Santa Cruz Biotech	sc-271834, RRID:AB_10707674	1/500 dilution
Antibody	Mouse anti-SHANK3	Santa Cruz Biotech	sc-30193, RRID:AB_2301759	1/1000 dilution

Resource Type	Specific Reagent or Resource	Source or Reference	Identifiers	Additional Information
Antibody	Streptavidin-HRP	R&D Systems	DY998	1/1000 dilution
Antibody	Mouse anti-SV2	DSHB	SV2, RRID:AB_2315387	1/3000 dilution
Antibody	Rabbit anti-SYNAPSIN1	Millipore	574777, RRID:AB_2200124	1/3000 dilution
Antibody	Mouse anti-SYNAPTOPHYSIN	Millipore	MAB5258, RRID:AB_2313839	1/2000 dilution
Antibody	Rabbit anti-SYNGAP1	Thermo Fisher Scientific	PA1-046, RRID:AB_2287112	1/2000 dilution
Antibody	goat anti-rabbit IgG-HRP	Santa Cruz	sc-2004, RRID: AB_631746	1/7000 dilution
Antibody	goat anti-mouse IgG-HRP	Santa Cruz	sc-2005, RRID: AB_631736	1/7000 dilution
Chemical Compound or Drug	5’ Biotin-dC-puromycin	Jena Bioscience	NU-925-BIO-S	
Chemical Compound or Drug	Cycloheximide	Sigma Aldrich	C7698	
Chemical Compound or Drug	Dithiothreitol	Sigma Aldrich	43815	
Chemical Compound or Drug	Complete EDTA-free protease inhibitor cocktail	Roche	11873580001	
Chemical Compound or Drug	Phosphatase Inhibitor Cocktail	Cell Signaling	5870	
Chemical Compound or Drug	Protease Inhibitor Cocktail	Sigma	P8340	
Chemical Compound or Drug	4x Laemmli Sample Buffer	Bio-Rad	1610747	
Chemical Compound or Drug	RNAsin RNase inhibitor	Promega	N2111	
Chemical Compound or Drug	IGEPAL CA-630	Sigma Aldrich	I8896	
Chemical Compound or Drug	QIAzol Lysis Reagent	Qiagen	79306	
Chemical Compound or Drug	luciferase spike-in control RNA	Promega	L4561	
Chemical Compound or Drug	TRIzol reagent	Thermo Fisher Scientific	15596026	
Chemical Compound or Drug	Dynabeads Protein G	Thermo Fisher Scientific	10003D	
Chemical Compound or Drug	CNQX	Tocris Bioscience	190	
Chemical Compound or Drug	Bicuculline	Tocris Bioscience	131	
Chemical Compound or Drug	Memantine hydrochloride	Sigma Aldrich	M9292	
Chemical Compound or Drug	D-Cycloserine	Abcam	ab120121	
Chemical Compound or Drug	D-amphetamine	Sigma Aldrich	A5880	

Resource Type	Specific Reagent or Resource	Source or Reference	Identifiers	Additional Information
Chemical Compound or Drug	A83-01	Stemcell Technologies	72022	
Chemical Compound or Drug	Dorsomorphin	Stemcell Technologies	72102	
Chemical Compound or Drug	Y-27632	Cellagen Technology	C9127-2s	
Chemical Compound or Drug	StemPro Accutase Cell Dissociation Reagent	Thermo Fisher Scientific	A1110501	
Chemical Compound or Drug	Dulbecco's Phosphate-Buffered Saline (DPBS)	Corning	21–031	
Chemical Compound or Drug	Dulbecco's Modification of Eagle's Medium (DMEM)	Corning	10–013	
Chemical Compound or Drug	DMEM/F-12, HEPES	Gibco	11330–032	
Chemical Compound or Drug	Neurobasal® Medium	Gibco	21103049	
Chemical Compound or Drug	KnockOut™ Serum Replacement	Gibco	10828028	
Chemical Compound or Drug	GlutaMAX™ Supplement	Gibco	35050061	
Chemical Compound or Drug	MEM Non-Essential Amino Acids Solution	Gibco	11140050	
Chemical Compound or Drug	Penicillin-Streptomycin (10,000 U/mL)	Gibco	15140122	
Chemical Compound or Drug	2-Mercaptoethanol	Gibco	21985023	
Chemical Compound or Drug	N-2 Supplement	Gibco	17502048	
Chemical Compound or Drug	B-27® Supplement	Gibco	17504044	
Chemical Compound or Drug	Matrigel® Growth Factor Reduced (GFR) Basement Membrane Matrix	Corning	354230	
Chemical Compound or Drug	Insulin solution	Sigma-Aldrich	I0516	
Chemical Compound or Drug	Fetal Bovine Serum (FBS)	Corning	35–010	
Chemical Compound or Drug	0.1% Gelatin in Water	Stemcell Technologies	7903	
Chemical Compound or Drug	Advanced DMEM/F-12	Gibco	12634010	
Chemical Compound or Drug	Human recombinant LIF	Stemcell Technologies	78055	
Chemical Compound or Drug	Costar® 6 Well Clear Flat Bottom Ultra Low Attachment plate	Sigma-Aldrich	CLS3471	
Chemical Compound or Drug	Recombinant Human FGF-basic	Peprotech	100–18B	
Chemical Compound or Drug	BDNF	Peprotech	450–02	
Chemical Compound or Drug	GDNF	Peprotech	450–10	

Resource Type	Specific Reagent or Resource	Source or Reference	Identifiers	Additional Information
Chemical Compound or Drug	Cyclopamine	Selleckchem	S1146	
Chemical Compound or Drug	Ascorbic acid	Sigma	1043003	
Chemical Compound or Drug	cAMP	Sigma	A6885	
Chemical Compound or Drug	SUPERase In RNase Inhibitor	Thermo Fisher Scientific	AM2694	
Chemical Compound or Drug	Pierce™ streptavidin magnetic beads	Thermo Fisher Scientific	88816	
Commercial Assay Or Kit	RNeasy Mini kit	Qiagen	74104	
Commercial Assay Or Kit	SuperScript III First-Strand Synthesis System	Thermo Fisher Scientific	18080051	
Commercial Assay Or Kit	Fast SYBR Green Master Mix	Thermo Fisher Scientific	4385610	
Commercial Assay Or Kit	NEBNext Ultra RNA Library Prep Kit for Illumina	New England Biolabs	E7530	
Cell Line	C1–1 (iPSC from normal human foreskin fibroblasts)	Yoon et al., 2014	N/A	
Cell Line	C1–2 (iPSC from normal human foreskin fibroblasts)	Yoon et al., 2014	N/A	
Cell Line	C3–1 (iPSC from normal human foreskin fibroblasts)	Yoon et al., 2014	N/A	
Cell Line	C3–2 (iPSC from normal human foreskin fibroblasts)	Yoon et al., 2014	N/A	
Cell Line	Y1–3 (iPSC from a fibroblast with 15q11.2 deletion)	Yoon et al., 2014	N/A	
Cell Line	Y1–4 (iPSC from a fibroblast with 15q11.2 deletion)	Yoon et al., 2014	N/A	
Cell Line	Y2–3 (iPSC from a fibroblast with 15q11.2 deletion)	Yoon et al., 2014	N/A	
Cell Line	Y2–4 (iPSC from a fibroblast with 15q11.2 deletion)	Yoon et al., 2014	N/A	
Organism/Strain	Mouse: B6.Cg-Tg(Nes-cre)1Kln/J	Jackson Laboratory	003771 RRID: IMSR_JAX:003771	
Organism/Strain	Mouse: *Cyfip1* floxed	This paper	N/A	
Organism/Strain	Mouse: *Cyfip1* conditional knock-in	This paper	N/A	
Recombinant DNA	qPCR primer_forward for mouse *Grin2a*:	This paper	N/A	
	GACCCCAAGAGCCTCATCAC			
Recombinant DNA	qPCR primer_reverse for mouse *Grin2a*:	This paper	N/A	
	CTGGATGGACGCTCCAAACT			
Recombinant DNA	qPCR primer_forward for mouse *Grin2b*:	This paper	N/A	
	TCTGACCGGAAGATCCAGGG			
Recombinant DNA	qPCR primer_reverse for mouse *Grin2b*:	This paper	N/A	
	TCCATGATGTTGAGCATTACGG			
Recombinant DNA	qPCR primer_forward for mouse *Shank2*:	This paper	N/A	

Resource Type	Specific Reagent or Resource	Source or Reference	Identifiers	Additional Information
	CTTTGGATTCGTGCTTCGAGG			
Recombinant DNA	qPCR primer_reverse for mouse *Shank2*:	This paper	N/A	
	GACTCCAGGTACTGTAGGGC			
Recombinant DNA	qPCR primer_forward for mouse *Psd95*:	This paper	N/A	
	TCGGTGACGACCCATCCAT			
Recombinant DNA	qPCR primer_reverse for mouse *Psd95*:	This paper	N/A	
	GCACGTCCACTTCATTTACAAAC			
Recombinant DNA	qPCR primer_forward for mouse *Homer1*:	This paper	N/A	
	CCGGGCAAACACCGTTTATG			
Recombinant DNA	qPCR primer_reverse for mouse *Homer1*:	This paper	N/A	
	TGCTAGTCGAGCAGCTTCTTTA			
Recombinant DNA	qPCR primer_forward for mouse *Synapsin1*:	This paper	N/A	
	AGTTCTTCGGAATGGGGTGAA			
Recombinant DNA	qPCR primer_reverse for mouse *Synapsin1*:	This paper	N/A	
	CAAACTGCGGTAGTCTCCGTT			
Recombinant DNA	qPCR primer_forward for mouse *Cyfip1*:	This paper	N/A	
	AACCCGAGGTCACAAAACTG			
Recombinant DNA	qPCR primer_reverse for mouse *Cyfip1*:	This paper	N/A	
	TTCAGCTCATCCAACACAGC			
Recombinant DNA	qPCR primer_forward for mouse *Grin1*:	This paper	N/A	
	TACAAGCGACACAAGGATGC			
Recombinant DNA	qPCR primer_reverse for mouse *Grin1*:	This paper	N/A	
	TCAGTGGGATGGTACTGC TG			
Recombinant DNA	qPCR primer_forward for mouse *Gria1*:	This paper	N/A	
	CGGAAATTGCTTATGGGACA			
Recombinant DNA	qPCR primer_reverse for mouse *Gria1*:	This paper	N/A	
	AC ACAGCGATTTTAGACCTCCT			
Recombinant DNA	qPCR primer_forward for human *GRIN2A*:	This paper	N/A	
	GACCCCAAGAGCCTCATCAC			
Recombinant DNA	qPCR primer_reverse for human *GRIN2A*:	This paper	N/A	
	CTGGATGGACGCTCCAAACT			
Recombinant DNA	qPCR primer_forward for human *GRIN2B*:	This paper	N/A	
	TCTGACCGGAAGATCCAGGG			
Recombinant DNA	qPCR primer_reverse for human *GRIN2B*:	This paper	N/A	
	TCCATGATGTTGAGCATTACGG			
Recombinant DNA	qPCR primer_forward for human *SHANK2*:	This paper	N/A	
	CTTTGGATTCGTGCTTCGAGG			
Recombinant DNA	qPCR primer_reverse for human *SHANK2*:	This paper	N/A	
	GACTCCAGGTACTGTAGGGC			

Resource Type	Specific Reagent or Resource	Source or Reference	Identifiers	Additional Information
Recombinant DNA	qPCR primer_forward for human *HOMER1*:	This paper	N/A	
	CCGGGCAAACACCGTTTATG			
Recombinant DNA	qPCR primer_reverse for human *HOMER1*:	This paper	N/A	
	TGCTAGTCGAGCAGCTTCTTTA			
Recombinant DNA	qPCR primer_forward for human *SYNAPSIN1*:	This paper	N/A	
	AGTTCTTCGGAATGGGGTGAA			
Recombinant DNA	qPCR primer_reverse for human *SYNAPSIN1*:	This paper	N/A	
	CAAACTGCGGTAGTCTCCGTT			
Software; Algorithm	Tophat2	Kim et al., 2013	https://ccb.jhu.edu/software/tophat/index.shtml	
Software; Algorithm	Fastx Toolkit	http://hannonlab.cshl.edu/fastx_toolkit	http://hannonlab.cshl.edu/fastx_toolkit/download.html	
Software; Algorithm	Toppgene	Chen et al., 2009	https://toppgene.cchmc.org	
Software; Algorithm	Webgestalt	Zhang et al., 2005	http://www.webgestalt.org/option.php	
Software; Algorithm	RIPSeeker	Li et al., 2013	https://bioconductor.org/packages/release/bioc/html/RIPSeeker.html	
Software; Algorithm	AnyMaze	Stoelting	http://www.anymaze.co.uk/index.htm	
Other	SuperSignal West Dura Extended Duration Substrate	Thermo Fisher Scientific	34075	
Other	Immun-Blot PVDF Membrane	Bio-Rad	1620177	
Other	2 ml Potter-Elvehjem Tissue Grinders	Thermo Fisher Scientific	358029	